Prestress evaluation in continuous PSC bridges by dynamic identification

Marco Breccolotti[*] and Francesco Pozza[a]

Department of Civil and Environmental Engineering, University of Perugia, 06125, Italy

Abstract.   In the last decades, research efforts have been spent to investigate the effect of prestressing on the dynamic behaviour of prestressed concrete (PSC) beams. Whereas no agreement has been reached among the achievements obtained by different Researchers and among the theoretical and the experimental results for simply supported beams, very few researches have addressed this problem in continuous PSC beams. This topic is, indeed, worthy of consideration bearing in mind that many relevant bridges and viaducts in the road and railway networks have been designed and constructed with this structural scheme.
In this paper the attention is, thus, focused on the dynamic features of continuous PSC bridges taking into account the effect of prestressing. This latter, in fact, contributes to the modification of the distribution of the bending stress along the beam, also by means of the secondary moments, and influences the flexural stiffness of the beam itself. The dynamic properties of a continuous, two spans bridge connected by a nonlinear spring have been extracted by solving an eigenvalue problem in different linearized configurations corresponding to different values of the prestress force. The stiffness of the nonlinear spring has been calculated considering the mechanical behaviour of the PSC beam in the uncracked and in the cracked stage. The application of the proposed methodology to several case studies indicates that the shift from the uncracked to the cracked stage due to an excessive prestress loss is clearly detectable looking at the variation of the dynamic properties of the beam. In service conditions, this shift happens for low values of the prestress losses (up to 20%) for structure with a high value of the ratio between the permanent load and the total load, as happens for instance in long span, continuous box bridges. In such conditions, the detection of the dynamic properties can provide meaningful information regarding the structural state of the PSC beam.

Keywords: prestressed continuous beams; bridge; prestress losses; non-destructive testing; dynamic properties

1. Introduction

Continuity has been introduced in road and railways bridges since '60. Whereas this type of construction is, generally, more complicated than simple span bridges, the reduction of the maintenance costs associated with bridge deck joints and deck drainage together with the improved riding qualities have contributed to the use of this construction technique on a large scale. Nowadays these structures continue to age and their assessment is becoming of primary interest.

∗Corresponding author, Ph.D., E-mail: marco.breccolotti@unipg.it
[a] M.Sc., E-mail: franch.p.3@gmail.com

Different technologies are available to monitor large infrastructures (Li *et al.* 2014) and specific procedures have been proposed for specific bridge types (e.g., Huang and Nagarajaiah 2014) but further research efforts should be placed on prestressed concrete bridges.

Regardless of the question whether the effect of prestressing, including secondary moments in statically indeterminate beams, should be taken into account only in service conditions or it should be considered at ultimate state conditions as well, there is no doubt about the need to assess the actual level of prestressing, especially in ageing existing structures. For this purpose, conventional techniques have been used by different Researchers. Remennikov and Kaewunruen (2015) used the dynamic relaxation technique to evaluate the prestressing force in prestressed concrete railways sleepers. Xuan *et al.* (2009) installed a monitoring system with optical fiber-sensors during the construction of a sewage treating tank aiming at evaluating the prestress force in the steel-strand. Both methods provide reliable estimate of the prestress force but their implementation requires, in the first case, some damage to the tested structure or, in the second case, the placement of the sensors during the construction stage.

NDE techniques have been recently used to assess prestress forces. Kim *et al.* (2010) used the stress wave's velocity that occurs when an impact is applied to a bonded tendon to evaluate its prestressing force. The experimental results demonstrate that the stress wave's velocity increases nonlinearly as the applied tensile force level is increased. The authors observed the same trend also on the effect of prestress in varying the concrete elastic modulus. Similar conclusions have been also drawn by Noble *et al.* (2016) based on the results of several experimental tests on PSC beams with different strand eccentricities that cause upward cambers. Conversely, diverse results have been obtained in the case of PSC beams where the effect of the eccentricity of the post-tensioning strand induced further cracking at the bottom fibre of the beam. Lundqvist and Rydén (2012) used resonant acoustic spectroscopy to measure the torsional and the longitudinal frequencies of vibrations of three prestressed concrete beams under different levels of prestressing force. The results of the experiments clearly showed that the measured resonance frequencies increased for higher compressive stress produced by the prestressing force.

Most of the investigations carried out so far on non-destructive techniques for the evaluation of the prestress force in PSC beams use dynamic identification techniques. Huang *et al.* (2011) analyzed the three-dimensional vibration behaviour of prestressed concrete bridges under moving vehicles using four-node isoparametric flat shell elements with transverse shear stiffness. The effect of prestress forces on the natural frequencies and on the dynamic response of the bridges was investigated by a step-by-step integration approach. According to their findings, the increase of the prestressing force yields a decrease in the natural frequencies and an increase in the time-dependent displacements of the bridge under moving loads. Similar numerical simulations were carried out by Li *et al.* (2013) to identify the magnitude of prestress force in a highway bridge by using the dynamic responses from moving vehicular loads. The unknown prestress force was iteratively identified from the measured structural dynamic responses by using an updating procedure based on the dynamic response sensitivity of a finite element model. Smail *et al.* (2014) proposed an inverse modeling technique that uses the dynamic strain responses and 2D elastodynamics to identify the pretension in the cable and the prestress in the concrete in a PSC beam. In their inverse technique, a classical data misfit function was minimized using a gradient-like algorithm identifying the stresses in the cable and in the concrete achieving an error smaller than 1% with only 4 iterations. Zhong *et al.* (2015) proposed a new bridge–vehicle model based on the principle of virtual work to investigate the interaction in terms of structural response between continuous prestressed bridges and vehicles with consideration of the prestress effect. The

model was validated by comparison with data available in the literature and with results of FE analyses. The conclusions indicate that prestress has a significant effect on the maximum vertical acceleration of the vehicles, which may provide a good index for detecting the change to the prestress force. Xiang *et al.* (2016) proposed a combination of 3 methods, the virtual distortion method, the Duhamel integral, and the load-shape function method to simultaneously identify the prestress force and the moving load acting on a PSC beam. Fang (2014) used the energy method to analyze the natural frequencies of externally PSC beams taking into account the second order effects and the compression softening phenomena. According to his findings, the compression softening effects vanishes progressively as the number of deviators increases from zero to a large number. It was also noticed that the eccentricity and the area of the tendon noticeably increase the 1st natural frequency of the simply supported beams. A general model able to take into account the effects of nonlinearity, softening, confinement and micro-cracking of concrete on the dynamic properties of simply supported PSC beams has been presented by Breccolotti (2018). The proposed model was applied with satisfactory results to four PSC beams with known mechanical and dynamic properties found in the literature.

From the experimental point of view, Limongelli *et al.* (2016) recently described the results of an experimental campaign carried out on a post-tensioned concrete beam with the aim of investigating the possibility of detecting, among other signs of deterioration, the increasing loss of prestress in the post tensioning cables. Based on the results of the tests, it was claimed that variations of the first and second modal frequencies with the tension in the prestressing cables are hardly detectable, unless the prestress loss induces the formation of a relevant cracking state. In this situation it must be also taken into account that cracks can open and close during vibration depending on the intensity of the external force that causes the vibration. This effect yields changes to the beam's flexural stiffness as reported by Breccolotti and Materazzi (2008) and by Breccolotti *et al.* (2008).

According to the above literature survey it can be noted that very few studies have been conducted on continuous PSC beams whereas this structural scheme has been frequently used in the context of important road and rail infrastructures for its enhanced structural performances in comparison to those of single span bridges. This paper therefore focuses on the evaluation of the dynamic properties of continuous PSC beams and particularly on the link between the frequencies of vibration and the level of prestress and on the ability to use the former for the assessment of the latter. This investigation is therefore motivated by the idea of using the dynamic characteristics as a quantitative indicator of the prestress force.

2. Eigenproperties of a two-span continuous beam with a nonlinear inner flexural spring

Dynamic identification has been widely investigated in the attempt of detecting damage at the earliest possible stage in civil, mechanical and aerospace engineering (Farrar and Jauregui 1998). Among different approaches, the flexibility method, based on the evaluation of the modal properties of the investigated structure, has been adopted.

The eigenproperties of a two-span continuous beam with a nonlinear flexural connection between the two spans (Fig. 1) can be derived from the classical free vibration equation according to the Euler-Bernoulli formulation with uniform cross section and negligible rotational inertia

$$\frac{\partial^4 v}{\partial x^4} + \frac{1}{EI}\rho\frac{\partial^2 v}{\partial t^2} = 0$$

(1)

where $v(x,t)$ is the transversal displacement, EI the bending stiffness and ρ the mass per unit length of the beam. With the variables separation method, the unknown displacement is written as

$$v(x,t) = \varphi(x)w(t)$$

(2)

The following solution can be obtained for each span

$$\varphi(x) = A_1\ sin(ax) + A_2\ cos(ax) + A_3\ sinh(ax) + A_4\ cosh(ax)$$

(3)

where the coefficients A_k depend on the boundary and continuity conditions. In this case, and when the flexural stiffness EI is uniform along the entire beam, the following conditions must hold

$$\begin{cases} \varphi_1(0) = 0 \\[2mm] \varphi''_1(0) = 0 \\[2mm] \varphi_1(L_1) = 0 \\[2mm] \varphi_2(0) = 0 \\[2mm] \varphi'_1(L_1) - \varphi'_2(0) = \frac{EI}{K_r}\varphi''_2(0) \\[2mm] \varphi''_1(L_1) = \varphi''_2(0) \\[2mm] \varphi_2(L_2) = 0 \\[2mm] \varphi''_2(L_2) = 0 \end{cases}$$

(4)

where the subscripts 1,2 refer to the first (left) and second (right) span, L_1 and L_2 are the lengths of the first and second span, respectively, and K_r is the stiffness of the nonlinear rotational spring that links the two spans at the inner support. Introducing Eq. (3) into Eq. (4) yields the following set of equations written in terms of the unknowns A_k
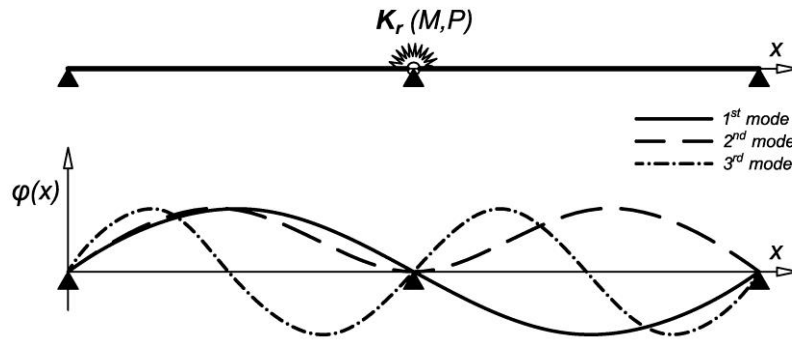
Fig. 1 Two-span continuous beam and nonlinear spring at the intermediate support (top) and first three mode shapes (bottom)

$$
\begin{cases}
A_1 + A_3 = 0 \\[2mm]
A_1 - A_3 = 0 \\[2mm]
A_2 \, sin(a \, L_1) + A_4 \, sinh(a \, L_1) = 0 \\[2mm]
A_5 + A_7 = 0 \\[2mm]
A_2 \, cos(a \, L_1) + A_4 \, cos h(a \, L_1) - A_6 - A_8 = \dfrac{E \, I}{K_r} a(-A_5 - A_7) \\[2mm]
-A_2 \, sin(a \, L_1) + A_4 \, sinh(a \, L_1) = -A_5 + A_7 \\[2mm]
A_5 \, cos(a \, L_2) + A_6 \, sin(a \, L_2) + A_7 \, cos h(a \, L_2) + A_8 \, sinh(a \, L_2) = 0 \\[2mm]
-A_5 \, cos(a \, L_2) - A_6 \, sin(a \, L_2) + A_7 \, cos h(a \, L_2) + A_8 \, sinh(a \, L_2) = 0
\end{cases}
\tag{5}
$$

After some trivial simplifications, this system of equations can be rewritten as

$$
\boldsymbol{M} \cdot \boldsymbol{A} = \boldsymbol{0}
\tag{6}
$$

where $\boldsymbol{M}$ is the coefficient matrix

$$M = \begin{bmatrix} 1 & 0 & 1 & 0 & 0 & 0 & 0 & 0 \\ 1 & 0 & -1 & 0 & 0 & 0 & 0 & 0 \\ 0 & s_{11} & 0 & s_{12} & 0 & 0 & 0 & 0 \\ 0 & 0 & 0 & 0 & 1 & 0 & 1 & 0 \\ 0 & c_{11} - \dfrac{EI}{K_r} a \cdot s_{11} & 0 & c_{12}(aL_1) + \dfrac{EI}{K_r} a \cdot s_{12} & 0 & -1 & 0 & -1 \\ 0 & -s_{11} & 0 & s_{12} & 1 & 0 & -1 & 0 \\ 0 & 0 & 0 & 0 & c_{21} & s_{21} & c_{22} & s_{22} \\ 0 & 0 & 0 & 0 & -c_{21} & -s_{21} & c_{22} & s_{22} \end{bmatrix}$$

(7)

with $s_{11} = sin(aL_1)$, $s_{12} = sinh(aL_1)$, $s_{21} = sin(aL_2)$, $s_{22} = sinh(aL_1)$,
$c_{11} = cos(aL_1)$, $c_{12} = cosh(aL_1)$, $c_{21} = cos(aL_2)$, $c_{22} = cosh(aL_1)$ with A the unknowns vector

$$A = \begin{bmatrix} A_1 & A_2 & A_3 & A_4 & A_5 & A_6 & A_7 & A_8 \end{bmatrix}^T$$

(8)

The homogeneous system of Eq. (6) has non-trivial solutions if the determinant of the coefficient matrix M vanishes. This condition yields a transcendental equation and its solutions a_n are determined numerically. The natural frequencies of the n-th mode can be calculated as

$$f_n = \frac{a_n^2}{2\pi} \sqrt{\frac{EI}{\rho}}$$

(9)

The mode shapes are schematically illustrated in Fig. 1. Depending on the value of the rotational stiffness K_r of the spring, different dynamic behaviors can be obtained. Specifically, if the value of K_r increases, the behavior gets closer to that of a continuous beam (no relative rotation of the two bays). If, conversely, the value of K_r decreases, the behavior tends to that of two simply supported beams connected by a hinge (null rotational stiffness) at the intermediate support. As will be shown later, in the present study it is hypothesized that the stiffness K_r of the connection between the two spans and, in turn, the dynamic properties of the beam, are nonlinear functions of the state of prestressing of the beam. Such a functional link is developed in the next section.

3. Influence of prestressing on the dynamic properties of the two-span PSC beams

The effect of prestressing on the dynamic properties of a continuous PSC beam is investigated with reference to a beam whose tendon profile is similar to the one reported in Naaman (2004). It is a two-span beam designed for a uniform service load distribution with the nonlinear tendon

profile shown in Fig. 2. It has to be highlighted that the permanent service load (the one that will be used in the evaluation of the dynamic properties of the beam) is naturally smaller than the loads used to check the safety of the beam at service and at ultimate conditions since it is hypothesized that variable loads, such as traffic, snow, etc., are not present during the execution of the dynamic tests.

The procedure to evaluate the effect of prestressing on the dynamic behaviour of the PSC beam can be summarized with the following steps:

1. Determination of the bending moment due to the beam self-weight, the superimposed loads and the prestressing force under the assumption that the beam is uncracked, linear, and elastic.

2. Determination of the nonlinear moment-curvature relationship for the beam cross-section with different values of axial force (corresponding to different values of prestress) in the cracked and uncracked state. In addition, determination of the bending moments $M_{cr}(P)$ that cause the cracking of the concrete for each different value of prestressing force P.

3. Determination, for each value of the prestressing force P, of the portion of the beam that is subjected to a bending moment greater than $M_{cr}(P)$ under the permanent service load.

4. Determination of the stiffness to be assigned to the rotational spring between the two spans according to the value of the prestressing force, the nonlinear moment-curvature relationship evaluated at step 2 and, eventually, the length of the cracked part of the beam.

5. Execution of dynamic analysis on the continuous beam composed by the two spans connected by the rotational spring and extraction of the free vibration frequencies and mode shapes for different values of the prestressing force.

These different steps are examined separately in the following. It must be pointed out that this procedure is certainly valid for post-tensioned unbonded prestressing strands. In fact, the occurrence of cracking due to an excessive prestress loss does not produce any meaningful increase in the prestressing force being the required strain increase in the prestressing steel averaged along the entire length of the beam. The procedure can be considered also valid for post-tensioned bonded prestressing strands. In this case concrete cracking is responsible of local strain increase in the prestressing steel with the consequent local increase in the prestressing steel stresses. Nevertheless, this effect is limited to the zone where cracking occurs and does not modify the loads equivalent to the prestressing.
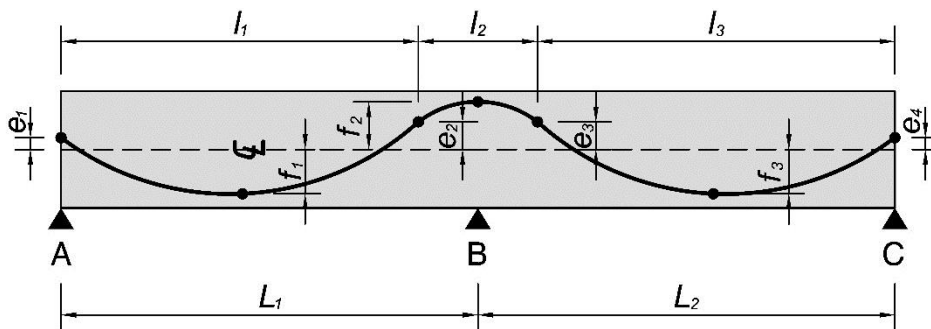
Fig. 2 Tendon profile (beam length not to scale)

3.1 Bending moment due to prestressing

While the effect of prestressing vanishes at ultimate states for the plastic deformation of the prestressing steel, it is still effective at permanent condition, thus influencing the distribution of the bending stresses along the beam. According to the standard procedure used in the design of prestressed beams, four equivalent systems of concentrated and distributed loads are introduced to replicate the effect of the prestressing force applied by the tendons. These latter are introduced by means of three parabolas, two of which with concavity upwards and one downwards, connected to each other to have the same tangent at the intersection point (Fig. 2). The equivalent loads exerted on the beam due to prestress are illustrated in Fig. 3.

The bending stresses produced by the forces equivalent to the prestressing are superimposed with those produced by the external load to obtain the overall bending moment diagram M. The effect of different values of the prestressing force (or, alternatively, the effect of prestress losses) can be argued looking at the example shown in Fig. 4.

3.2 Nonlinear moment – curvature relationship for prestressed sections

The relationship between the bending moment and the corresponding curvature for a beam having a rectangular cross section and subjected to a compressive force P equal to the prestressing force is analyzed assuming a plastic behaviour of the prestressing strand and the reinforcement rebar and nonlinear constitutive relation for the concrete in compression proposed by Park and Paulay (1975)

$$\sigma_{c,c}\left(\varepsilon_c\right) = f_{ck}\left[\frac{2\varepsilon_c}{\varepsilon_0} - \left(\frac{\varepsilon_c}{\varepsilon_0}\right)^2\right] \tag{10}$$
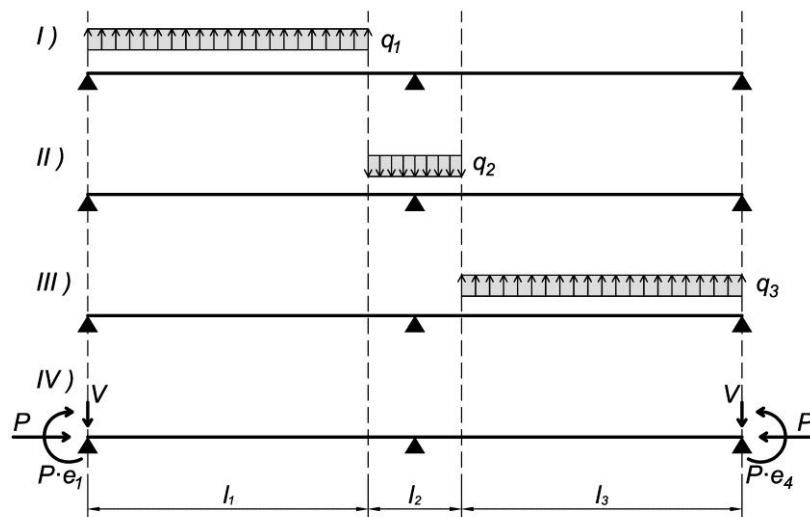
Fig. 3 Prestressing equivalent loads
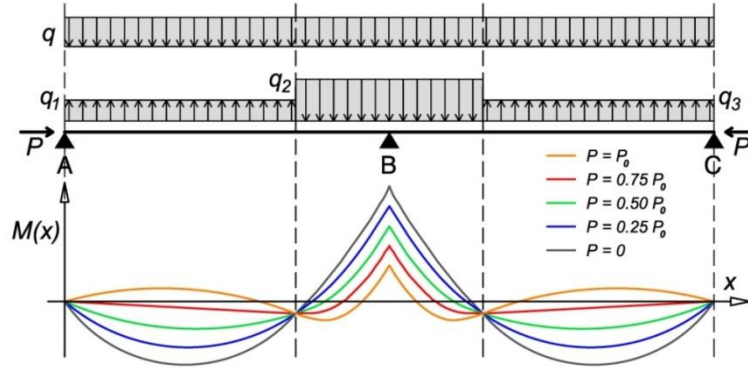
Fig. 4 External loads, prestressing equivalent loads and overall bending moment for different values of the prestressing force

where $\sigma_{c,c}$ is the compressive stress in the concrete (positive), f_{ck} is the concrete characteristic compressive strength, ε_c is the concrete strain (positive in contraction), and $\varepsilon_0 = 2‰$. For concrete in tension, a linear elastic behaviour is assumed up to cracking

$$\sigma_{c,t}\left(\varepsilon_c\right) = \varepsilon_t\, E_{c,0} \tag{11}$$

with

$$E_{c,0} = \left.\frac{d(\sigma_{c,c})}{d\varepsilon_c}\right|_{\varepsilon_c = 0} = 2\frac{f_{ck}}{\varepsilon_0} \tag{12}$$

and where $\sigma_{c,t}$ is the tensile stress in the concrete (negative), ε_t is the concrete strain and $E_{c,0}$ is the tangent elastic modulus of the concrete at the origin. The complete stress-strain diagram for the concrete is displayed in Fig. 5(a). It is assumed that cracking of the concrete occurs when its strain reaches the value

$$\varepsilon_{c,t} = \frac{f_{cfm}}{E_{c,0}} \tag{13}$$

with f_{cfm} mean tensile strength for bending stresses of the concrete (CEN 2014).

For the reinforcement, steel type B450C (CEN 2014) is assumed. The stress-strain relation for the steel reinforcement is assumed linear up to yielding, both in compression and in tension (Fig. 5(b))

$$\sigma_a\left(\varepsilon\right) = \varepsilon\, E_s \tag{14}$$
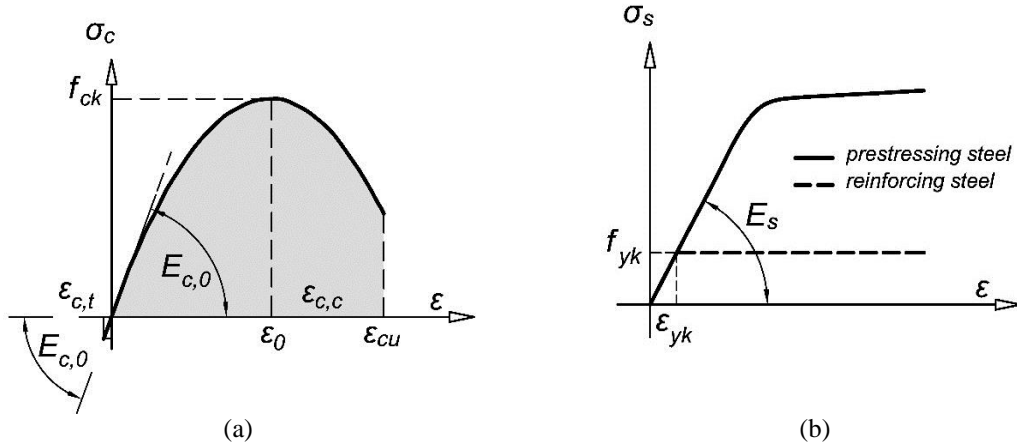
Fig. 5 (a) Concrete stress-strain relationship and (b) Prestressing and reinforcing steels stress-strain relationships
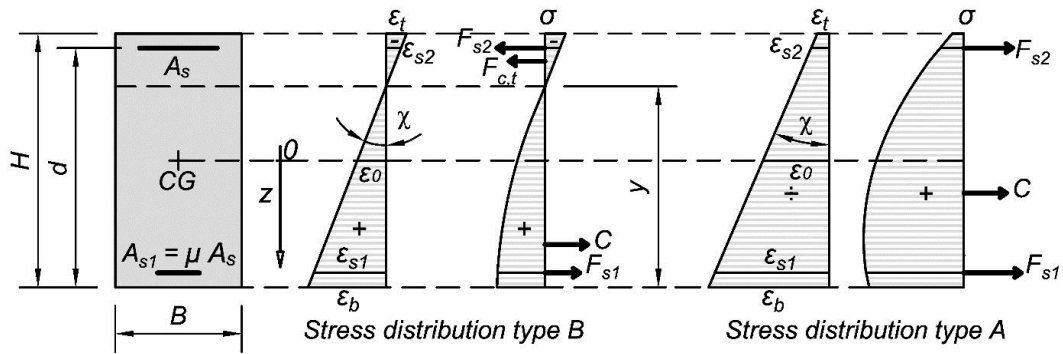
Fig. 6 Strain and stress distributions in the uncracked stage

where σ_a is the stress in the steel and E_s is its elastic modulus. The latter is taken as 200 GPa.

The variation of the bending stiffness for different prestressing forces is examined separately for the uncracked and the cracked stages. In the first case, the concrete contributes to the stiffness along the entire region. In the second case, the cracking that occurs in the concrete at discrete locations yields a reduction in the overall flexural stiffness. In the following, we will refer to a rectangular section with dimension B and H, an area of steel in tension A_S and an area of steel in compression $A_{S1} = \mu \cdot A_S$ (Fig. 6).

3.2.1 Uncracked stage

In the uncracked stage of a PSC beam, two different distributions of stresses can occur: a distribution with only compression stresses (type A) and a distribution with both, compression and tensile stresses (type B) as depicted in Fig. 6.

A closed form expression for the internal bending stress distribution can be obtained for both types as a function of the curvature χ and of the prestressing value P

$$M_{R,A} = M_{R,A}(\chi, P) \tag{15}$$

$$M_{R,B} = M_{R,B}(\chi, P) \tag{16}$$

From these relationships it is possible to determine the bending stiffness of the cross section by means of the derivative of the bending moment with respect to the curvature χ. The cross sectional flexural stiffnesses turn out to be function of the prestressing force P and of the bending moment acting on the section M_R

$$k_{e,A} = \frac{d(M_{R,A})}{d\chi} \tag{17}$$

$$k_{e,B} = \frac{d(M_{R,B})}{d\chi} \tag{18}$$

As will be shown later in the case studies, it is interesting to note that in the uncracked stage the bending stiffness slightly increases with increasing values of the prestressing forces. This can be ascribed to the softening behaviour of the concrete that becomes more deformable for increasing compressive stresses.

3.2.2 Cracked stage
In the cracked stage the attainment of the concrete tensile strength divides the beam cross-sections into two parts (Fig. 7). The curvature χ_{II} that defines the shift from the uncracked stage to the cracked one is equal to.

$$\chi_{II} = \frac{\varepsilon_{c,t,max}}{(H - y)} \tag{19}$$

where $\varepsilon_{c,t,max}$ is the strain of the concrete corresponding to its tensile strength and y is the height of the compressed part of the section from the most stressed fibre to the neutral axis (Fig. 7). By introducing Eq. (19) into Eq. (16) it is possible to obtain the relation between the cracking moment M_{cr} and the prestressing force P

$$M_{cr} = M_{R,B}\big|_{\chi = \chi_{II}} \tag{20}$$

The behaviour of the cracked section is investigated up to the tensile yielding of the reinforcement since is of very little interest considering the case of yielded steel rebars. This means that the strain in the tensile steel is investigated up to the value (Fig. 5)

$$\varepsilon_{sn} = -\frac{f_{yk}}{E_s} \tag{21}$$

and, correspondingly, the curvature is analyzed up to the value

$$\chi_{sn} = \frac{\varepsilon_{sn}}{(d-y)} \tag{22}$$

Also in this case a closed form formulation has been derived for the internal moment and for the flexural stiffness

$$M_{R,II} = M_{R,II}(\chi, P) \tag{23}$$

$$k_{cr} = \frac{d(M_{R,II})}{d\chi} \tag{24}$$

3.3 Evaluation of the flexural stiffness in the cracked part of the beam

The length of the cracked part of the beam is designated by l_{cr}. In this region, the bending moment, which is larger than the cracking one, M_{cr}, yields tensile stresses that exceed the concrete tensile strength and trigger the formation of cracks (Fig. 8(a)). In this part of the beam, neither the flexural stiffness of the cracked stage nor that of the uncracked stage correctly represents the effective flexural stiffness. In fact, in a well-developed cracking pattern (see Fig. 8(b)), there are parts of the beam where the stiffness is reduced while there are other parts located between every couple of consecutive cracks where the beam is almost undamaged.

An evaluation of the flexural stiffness of the cracked region is carried out according to the relations proposed by Ghosh and Khuntia (2004a, b) on the basis of parametric studies on the moment of inertia of reinforced concrete columns and beams. In fact, if the prestressing action is significant, the cross sectional flexural stiffness of the PSC beam is similar to that of reinforced concrete column

$$k_{eff} = E_c I (0.80 + 25\rho_{tot}) \left(1 - \frac{e}{h} - 0.5\frac{P}{P_u}\right) \le E_c I \tag{25}$$

where ρ_{tot} is the ratio of the total reinforcement area over the concrete cross section area, E_c is the elastic modulus of the concrete, I is the moment of inertia of the cross section, the eccentricity e is the ratio of the total bending moment M and the prestressing force P, and P_u is the ultimate strength in compression of the concrete section without bending moments. Conversely, if the prestressing action is small, the flexural stiffness of the PSC beam is similar to that of reinforced concrete beam

$$k_{eff} = E_c I (0.10 + 25\rho_{tensile}) \left(1 - 0.2\frac{B}{H}\right) \le 0.60 E_c I \tag{26}$$

where B and H represent width and height of the section, respectively, and $\rho_{tensile}$ is the ratio of the tensile reinforcement area over the concrete cross section area.
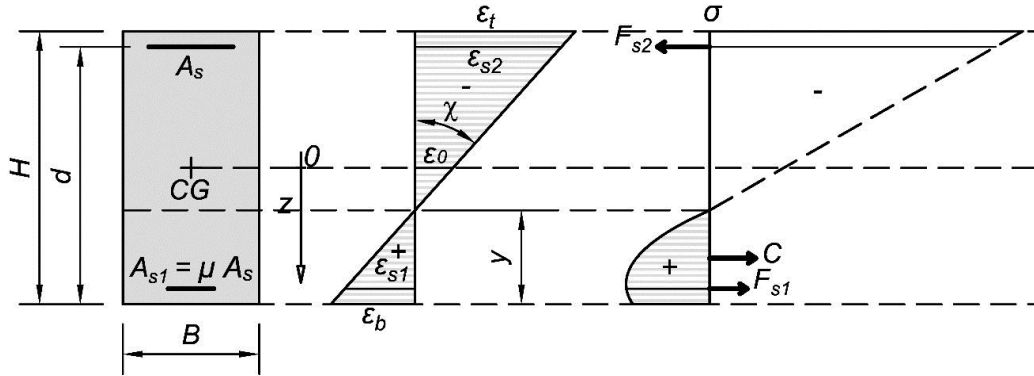
Fig. 7 Strain and stress distributions in the cracked stage

(a)   (b)
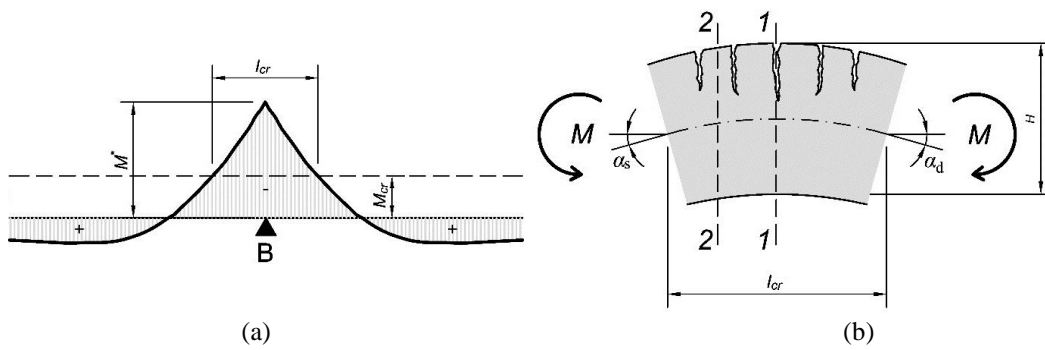
Fig. 8 Finite length cracked zone of a PSC beam: a) bending moment and (b) cracking pattern.

The relative rotation θ between the two ends of a cracked region of the beam with length l_{cr} and flexural stiffness k_{eff} under a uniform bending moment M with $M^* < M < M_{cr}$ is equal to

$$\theta = \frac{M}{k_{eff}} l_{cr}$$

(27)

where M is the averaged bending moment along the cracked region and θ can also be written as $\theta = \alpha_s + \alpha_d$ (Fig. 8(b)).

As discussed in the previous paragraphs, the assessment of the flexural stiffnesses of the cracked and the uncracked sections of a RC beam can be achieved using Eqs. (17), (18), (25), (26).

Opposed to that, calculating the flexural stiffness of a finite length part of a cracked RC beam with length l_{cr} is not so straightforward. It can however be taught of as the combination of two contributions: that of the cracked sections (sections type 1-1 in Fig. 8(b)) with a bending stiffness k_{cr} that takes into account the concrete partialization and the nonlinear behaviour of the concrete

in compression, and that of the uncracked sections k_e (sections type 2-2 in Fig. 8(b)) that takes into account the nonlinear behaviour of the concrete in compression. Thus, it can be assumed that the overall relative rotation $\theta(k_{eff})$ is the sum of the rotations occurring in two consecutive homogeneous finite length beams that correspond to the uncracked and the cracked parts, with cross sectional stiffnesses k_e and k_{cr}

$$\theta(k_{eff}) = \theta(k_e) + \theta(k_{cr}) \tag{28}$$

Assuming that within the length l_{cr} the portion of the uncracked sections is equal to a while the length of the cracked sections is equal to b and that both parts are subjected to the same bending moment M, the following system of equations in the unknowns a and b can be written

$$\begin{cases} \dfrac{M}{k_{eff}} l_{cr} = \dfrac{M}{k_e} a + \dfrac{M}{k_{cr}} b \\[2mm] l_{cr} = a + b \end{cases} \tag{29}$$

By using the values for k_{eff} given in Eqs. (25) and (26), which depends on the bending moment M and prestressing force P, the system of Eq. (29) can be solved for the following unknowns

$$a = \frac{l_{cr}\left(\dfrac{1}{k_{eff}} - \dfrac{1}{k_{cr}}\right)}{\left(\dfrac{1}{k_e} - \dfrac{1}{k_{cr}}\right)} \tag{30}$$

$$b = l_{cr} - a \tag{31}$$

The effective flexural stiffness used for the cracked portion of the beam can, thus, be rewritten as

$$k_{eff} = \frac{l_{cr} \cdot k_e \cdot k_{cr}}{a \cdot k_{cr} + b \cdot k_e} \tag{32}$$

In the study of the dynamic behavior of the PSC beam, the assumption of concentrated plasticity lumps the effect of the cracked region to a point located at the inner support (point B in Fig. 4) and represented by the rotational spring. The stiffness of the rotational spring K_r is then equivalent to the stiffness of the cracked part of the beam

$$K_r(\theta) = \frac{k_{eff}}{l_{cr}} \tag{33}$$

3.4 Eigenfrequencies and mode shapes

Eigenfrequencies and mode shapes of the nonlinear two-span continuous beam are extracted from the structure by linearizing its behaviour in the neighborhood of the equilibrium point reached following the application of the permanent loads and of the investigated value of prestress force. The following procedure is coded in a Maple environment for the evaluation of the influence of the prestress force on the dynamic properties of a PSC beam:

1. Definition of a set of values of the prestress force P in the range between 0 and the initial prestress force P_0 for which the dynamic properties of the beam are evaluated;
2. Calculation of the distributions of bending stresses produced by the external loads in service condition and by the different values of the prestressing forces;
3. Determination of the rotational spring stiffness K_r equivalent to the portion of beam connecting the two spans for each value of the prestressing force P (Eq. (31));
4. Implementation of the values K_r in the coefficients matrix M and calculation of the values a_n that nullify the determinant of the matrix for each value of P;
5. Determination of the unknowns $A_1, ..., A_8$ of the linear system in Eq. (6) and subsequent identification of the mode shapes for each value of P;
6. Determination of the eigenfrequencies (Eq. (7)) for each value of the prestressing force.

Repeating steps 1-6 for the whole series of prestressing forces (defined here as a percentage of the initial reference force P_0 defines the link between the level of prestress and the frequencies of vibration. The inverse form of this link allows assessing the level of prestress based on measurement of the natural frequencies.

It must be pointed out that, at the actual stage of research, the evaluation of the bending moment distributions mentioned at point 2) is carried out neglecting the variation of the flexural stiffness at point B consequent to the variation of the prestressing force.

4. Case studies

The procedure presented in the previous section is applied to three case studies of continuous PSC beams with two spans and a piecewise parabolic cable. The first and the third ones correspond to a beam with two equal length spans while the beam studied in the second case has two spans with different lengths. The geometrical features of the beams and of the cable layouts are summarized in Table 1 (see Fig. 2 for the notations). The dimension of the beams cross sections and the amount of reinforcements are listed in Table 2 with the notations of Fig. 6. The mechanical properties of the materials used for the three case studies are reported in Table 3.

4.1 Case study I: continuous PSC beam with 2 equal spans and low level of live load

The first case studies a 50 m long PSC beam with two 25 m long spans. The design loads include the beam's self-weight, $G_1 = 15$ kN/m, the superimposed dead load, $G_2 = 30$ kN/m, and the live load, $Q_1 = 15$ kN/m.

The minimum prestressing force for the section at the internal support can be preliminarily calculated neglecting the secondary moments by using the Magnel diagram (Magnel 1951) and

Table 1 Geometrical features of the beam and of the cable layout for the three case studies

Case study	L_1	L_2	l_1	l_2	l_3	e_1	e_2	e_3	e_4	f_1	f_2	f_3
	(m)	(m)	(m)	(m)	(m)	(mm)	(mm)	(mm)	(mm)	(mm)	(mm)	(mm)
I	25	25	18.75	12.5	18.75	0	200	200	0	600	600	600
II	30	15	22.5	15	7.5	0	200	200	0	600	600	600
III	25	25	18.75	12.5	18.75	0	200	200	0	600	600	600

Table 2 Dimension of the beams cross sections and amount of reinforcements for the three case studies

Case study	H	B	d	A_S	A_{S1}	A_P
	(mm)	(mm)	(mm)	(mm^2)	(mm^2)	(mm^2)
I	1500	400	1350	1005	1005	4200
II	1500	400	1350	1005	1005	4200
III	1500	400	1350	1005	1005	4200

Table 3 Physical and mechanical properties of materials

Material	Property	Symbol	Value	u.m.
Concrete	Characteristic cylindrical compressive strength	f_{ck}	35.0	MPa
	Mean tensile strength	f_{ctm}	3.21	MPa
	Compressive strain at maximum stress	ε_0	0.0020	--
	Ultimate compressive strain	ε_{cu}	0.0035	--
	Ultimate tensile strain	ε_{ct}	0.0001	--
Steel	Characteristic tensile strength	f_{yk}	450	MPa
	Elastic modulus	E_s	200	GPa
	Characteristic yielding strain	ε_{yk}	0.00225	--

assuming the maximum practical eccentricity and the attainment of the concrete tensile strength at the extrados under the minimum (negative) bending moment

$$\eta P_0 = \frac{|M_{min}| + \overline{\sigma_{ts}} Z_t}{e_0 - k_b} \tag{34}$$

where M_{min} is the moment produced by the unfactored dead and live loads, η is a coefficient that introduces the prestress losses at a preliminary stage, $\overline{\sigma_{ts}}$ is the admissible concrete tensile stress, Z_t is the section modulus with respect to the top fiber, k_b is the distance from the centroid of the concrete section to the lower limit of the central kernel and e_0 is the eccentricity of the prestressing steel with respect to the centroid of the concrete section. For the sake of simplicity, an initial prestressing force P_0 equal to 4200 kN is assumed for each case study.
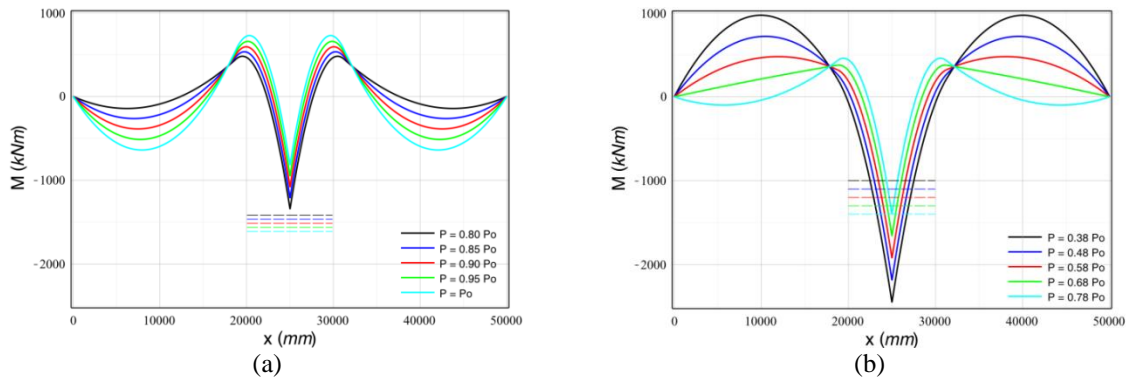
Fig. 9 Case study I – Bending moments (solid lines) and cracking moments (dashed lines) for different values of the prestressing force in the uncracked stage (a) and in the cracked stage (b)

To simulate the condition of a hypothetical dynamic test, the live load is not considered in the calculation of the bending moment distribution along the PSC beam and in the evaluation of the corresponding dynamic properties. The distributions of the bending moment for different values of the prestressing force are shown in Fig. 9. In this figure, the cases of the uncracked stages are shown in the left part while those of the cracked stages are shown in the right side. The diagrams of the bending moments are shown with solid curves while the cracking moments are shown with dashed lines. A different colour is used for each value of the prestress force. From the right figure, the length of the cracked portion that corresponds to each values of the prestress force can also be determined. These lengths are reported in Table 4.

Based on the analyses described in the previous section, the relationship between the bending moment M and the flexural stiffness K for the uncracked and cracked section and for different values of the prestressing force is determined. These relationships are shown in Fig. 10. In the figure the solid circles designate the bending moments occurring in the nonlinear beam at the internal support (point B of Fig. 4) for different values of the prestress force. It can be observed that:

1. a decrease in the prestress force yields an increase in the bending moment in the section at the internal support;

2. the decrease of the prestress force combined with the increase of the bending moment in the uncracked stage produces a slight increase of the bending stiffness. This slight increase is associated with negligible variations of the dynamic properties of the prestressed beam. This result is similar to that found for simply supported beams by Hamed and Frostig (2004);

3. the decrease of the prestress force combined with the increase of the bending moment in the cracked stage produces a significant reduction of the bending stiffness. This result is similar to that obtained by Hamed and Frostig (2006) who observed a significant reduction of the natural frequencies of simply supported PSC beams following the cracking induced by increasing external loads.

In the uncracked stage, a prestress reduction of 20% produces an increase of section flexural stiffness of 4.0%. In the cracked stage, conversely, a decrease of prestress from 0.78 P_0 to 0.68

P_0 is responsible for a 40% reduction of the flexural stiffness. This flexural stiffness is used according to par. 3.3 to calculate the stiffness of the rotational spring for the eigenvalues analyses.

The first four frequencies of vibration calculated for the investigated values of the prestress force are shown in Fig. 11 for the uncracked and cracked stage. In this figure, the variations of the eigenfrequencies f_i (normalized with respect to the frequencies f_{i,P_0} are plotted as a function of the relative reduction of the prestress force $(P - P_0)/P_0$). It can be observed that the slight variation of the bending stiffness of the nonlinear portion is not sufficient to trigger significant variations in the dynamic properties of the PSC beam in the uncracked stage. Conversely, relevant variations of the 2nd and the 4th frequency of vibrations are foreseen in the cracked stage. As expected in this case, the 1st and the 3rd mode are not affected by the value of the prestress loss. This is due to the zero curvature of the cracked portion of the beam in those modes. The frequency of vibrations and the mode shapes in the cracked stage are reported in the Table 5 and in Fig. 12, respectively. Fig. 13 shows the relative variations between the normalized 2nd and 4th mode shapes corresponding to the initial value of the prestress force (P_0) and to a prestress force equal to 0.68 P_0. These values have been calculated for the i-th mode shape φ_i as follow

$$\frac{\varphi_i^{P=P_0}(x) - \varphi_i^{P=0.68P_0}(x)}{\varphi_i^{P=P_0}(x)} \tag{35}$$

Even if the relative variations of the mode shapes turned out to be not negligible in the present work, only the eigenfrequencies will be used to assess the prestress force for their higher reliability and ease of measurement.

For the present case, dynamic tests can be considered of great utility since they are able to identify cracking and monitor the evolution of the prestress forces starting from a value of 0.78 P_0, which is roughly equal to that considered in the design process. This possibility is relevant since cracking produced by excessive prestress loss or by tendon rupture is not easily detectable in continuous PSC bridges by visual inspection occurring, generally, at the extrados under the asphalt layer. The use of a limited number of sensors with a continuous monitoring system would, instead, be able to detect this type of damage.

(a)   (b)
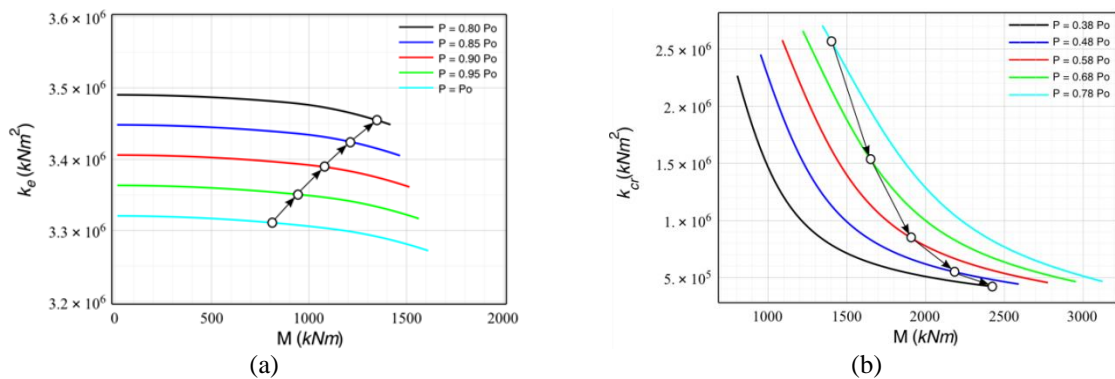
Fig. 10 Case study I - Variation of the flexural stiffness as a function of the bending moment and prestressing force in the uncracked stage (a) and in the cracked stage (b)

Table 4 Case study I - Length of cracked part of PSC beam for different values of prestressing force

P/P_0	P [kN]	l_{cr} [mm]	K_r [kN m]
0.78	3276	2	$1.280 \cdot 10^9$
0.68	2856	1105	$2.920 \cdot 10^6$
0.58	2436	2299	$1.451 \cdot 10^6$
0.48	2016	3572	$9.435 \cdot 10^5$
0.38	1596	4899	$6.438 \cdot 10^5$

Table 5 Case study I - First 4 frequencies of vibration for different values of prestressing force (cracked stage)

P/P_0	P [%]	P [kN]	f_1 (Hz)	f_2 (Hz)	f_3 (Hz)	f_4 (Hz)
0.78	22	3276	2.2357	3.4975	8.9524	11.3304
0.68	32	2856	2.2357	3.3457	8.9524	10.8751
0.58	42	2436	2.2357	3.2255	8.9524	10.5557
0.48	52	2016	2.2357	3.1243	8.9524	10.3122
0.38	62	1596	2.2357	3.0168	8.9524	10.0813
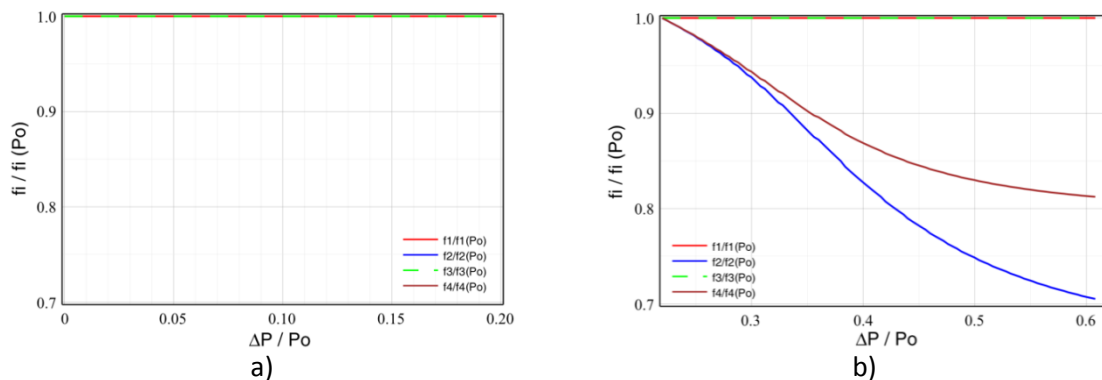
Fig. 11 Case study I - Relative variations of the first 4 frequencies of vibration for decreasing values of the prestress force in the uncracked stage (a) and in the cracked stage (b)

4.2 Case study II: continuous PSC beam with two unequal length spans

The second case study deals with a PSC beam on three supports with an overall length of 45 m. The length of the first span equals 30 m while the other one equals 15 m forming an asymmetric structure. The path of the nonlinear cable is described by the data in Tab. 1. The geometrical and physical characteristics of the rectangular section are the same as the ones used in the previous case study (Tables and 3). The design loads include the beam's self-weight, G_1=15 kN∕m, the superimposed dead load G_2=20 kN∕m and the live load Q_1=10 kN∕m. Also in this case, the

resulting initial prestressing force P_0 equals 4200 kN. Fig. 14 shows the bending moments (continuous curves) and the cracking moment at the internal support (dashed lines) for different values of the prestressing force in the uncracked and in the cracked stages. The lengths of the cracked region of the PSC beam in the vicinity of the internal support are shown in Table 6 for the investigated values of effective prestress forces. In this case, cracking occurs at the internal support as a consequence of a prestress degradation of approximately 23%. The variation of the flexural stiffness as a function of the bending moment and prestressing force in the uncracked and in the cracked stages are shown in Fig. 15. Similarly to case study I, in the uncracked stage, a prestress force of 0.8 P_0 yields an increase of the section's flexural stiffness of 4.3% while in the cracked stage, an decrease of prestress force from 0.77 P_0 to 0.66 P_0 yields a 41% reduction of the flexural stiffness. In this case, the changes to the prestress force affect the first, third, and fourth eigenfrequencies (Table 7) in the cracked stage while its influence is negligible in the uncracked stage. The variations of the normalized frequencies of vibration f_i as a function of prestress force, shown graphically in Fig. 16, reach a maximum value of 5% for the 3rd mode for prestress decreasing from a value of 0.77 P_0 to 0.67 P_0.

4.3 Case study III: continuous PSC beam with 2 equal spans and high live load

The third case study uses the same geometry and the same total load of the first one, but with a higher level of live load: beam selfweight G_1 =15 kN/m, superdead load G_2 =20 kN/m and live load Q_1 =25 kN/m.

Table 6 Case study II - Length of cracked part of PSC beam for different values of prestressing force

P/P_0	P [kN]	l_{cr} [mm]	K_r [kN m]
0.77	3234	31	$9.743 \cdot 10^7$
0.66	2772	1357	$2.378 \cdot 10^6$
0.55	2310	2838	$1.174 \cdot 10^6$
0.44	1848	4475	$7.520 \cdot 10^5$
0.33	1386	6241	$5.055 \cdot 10^5$

Table 7 Case study II - First 4 frequencies of vibration for different values of prestressing force (cracked stage)

P/P_0	P [%]	P [kN]	f_1 (Hz)	f_2 (Hz)	f_3 (Hz)	f_4 (Hz)
0.77	23	3234	2.2579	7.0487	9.8410	17.3103
0.66	34	2772	2.1978	7.0487	9.3003	16.9213
0.55	45	2310	2.1503	7.0487	8.9145	16.6842
0.44	56	1848	2.1092	7.0487	8.6109	16.5166
0.33	67	1386	2.0618	7.0487	8.3294	16.3743
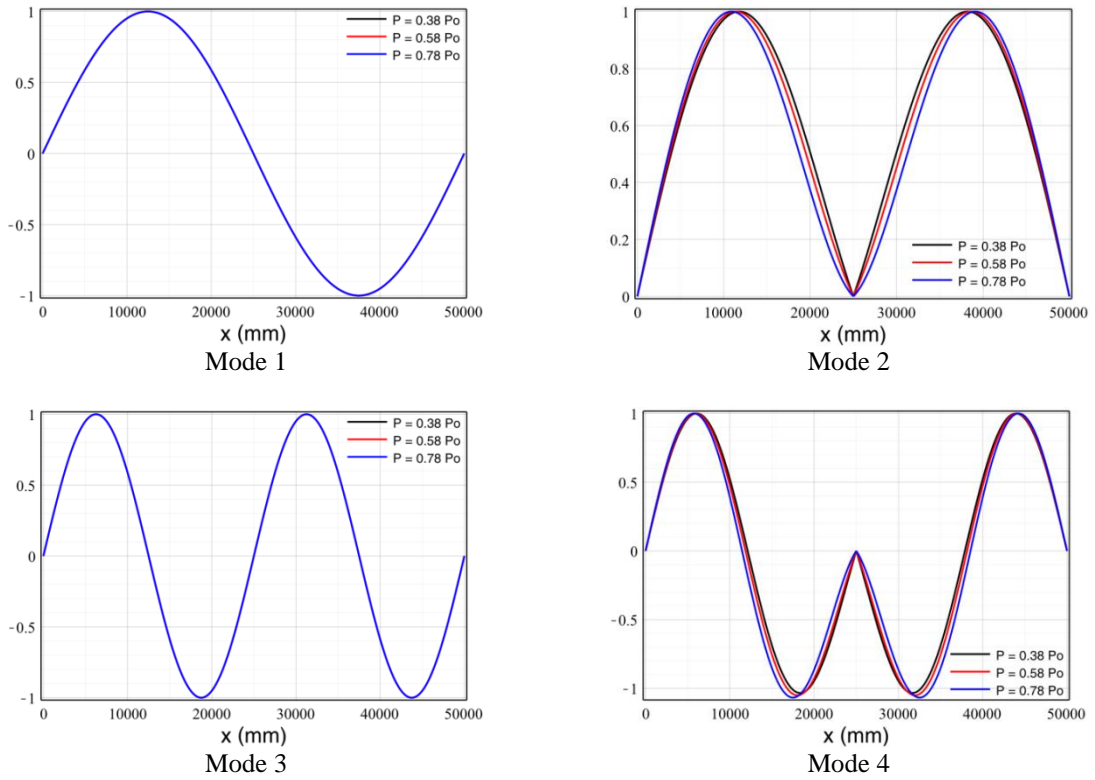
Fig. 12 Case study I - First 4 mode shapes for decreasing values of the prestress force in the cracked stage
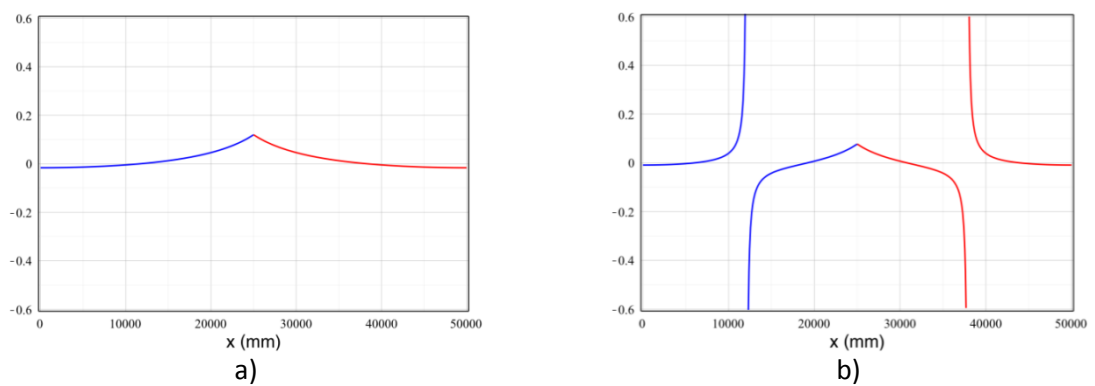
Fig. 13 Case study I - Relative variations between mode shapes corresponding to $P = P_0$ and $P = 0.68 P_0$ for the 2nd (a) and the 4th mode shape (b)
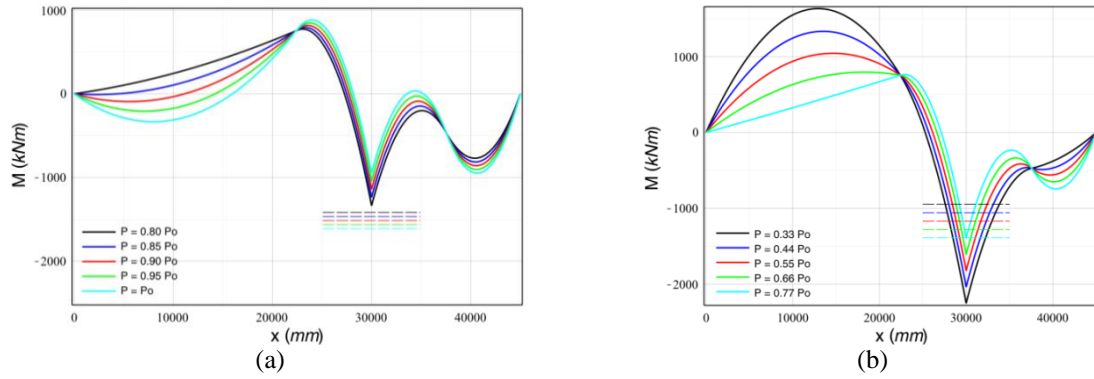
Fig. 14 Case study II – Bending moments (solid lines) and cracking moments (dashed lines) for different values of the prestressing force in the uncracked stage (a) and in the cracked stage (b)
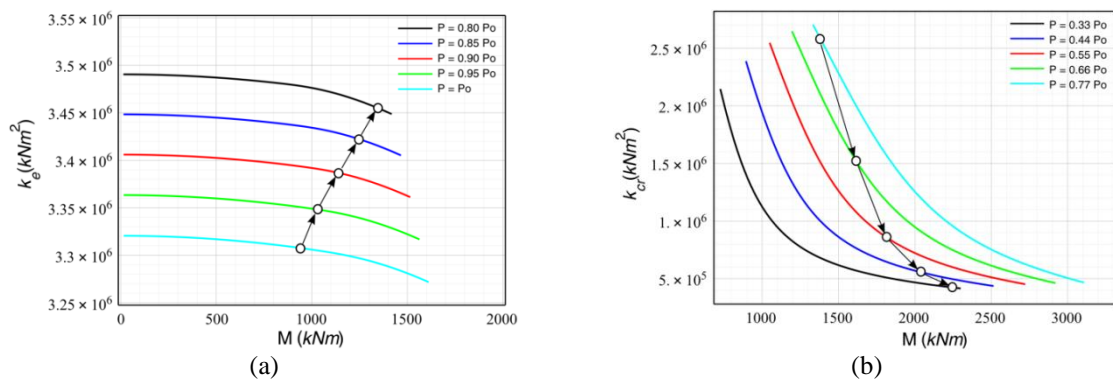
Fig. 15 Case study II - Variation of the flexural stiffness as a function of the bending moment and prestressing force in the uncracked stage (a) and in the cracked stage (b)
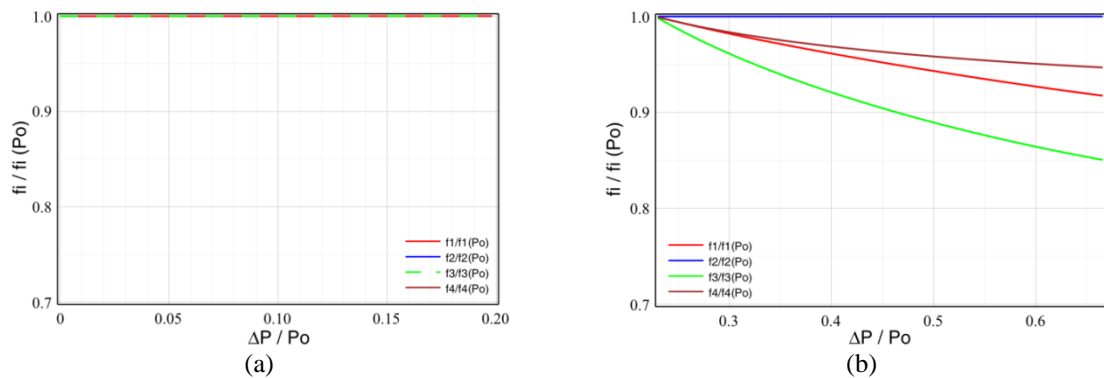
Fig. 16 Case study II - Relative variations of the first 4 frequencies of vibration for decreasing values of the prestress force in the uncracked stage (a) and in the cracked stage (b)

Since the total load is the same as in the first case study, the same prestressing force of case I is used here as well. Nevertheless, as already mentioned, the determination of the dynamic properties is carried out assuming quasi-permanent conditions, thus neglecting the relevant live load. Under this condition, cracking at the intermediate support occurs for a prestress force of 0.58 P_0 (Fig. 17). This very high value indicates that a PSC beam designed for high live loads can undergo significant prestress reduction in service condition prior to cracking. The variation of the flexural stiffness as a function of the bending moment and prestressing force (Fig. 18) follows trends that are similar to those observed in the first case study, though for different values of the prestress force. Similar observations can be made, also, for the relative variations of the first 4 frequencies of vibration for decreasing values of the prestress force (Fig. 19). In this case the dynamic tests can be considered of little utility since they may detect cracking and monitor the evolution of the prestress forces only after a significant change of the prestress force.

Table 8 Case study III - Length of cracked part of PSC beam for different values of prestressing force

P/P_0	P [kN]	l_{cr} [mm]	K_r [kN m]
0.56	2352	119	$2.582 \cdot 10^7$
0.48	2016	1297	$2.531 \cdot 10^6$
0.40	1680	2566	$1.303 \cdot 10^6$
0.32	1344	3907	$8.588 \cdot 10^5$
0.24	1008	5283	$5.971 \cdot 10^5$

Table 9 Case study III - First 4 frequencies of vibration for different values of prestressing force (cracked stage)

P/P_0	P [%]	P [kN]	f_1 (Hz)	f_2 (Hz)	f_3 (Hz)	f_4 (Hz)
0.56	44	2352	2.5393	3.3836	10.1509	11.3842
0.48	52	2016	2.5393	3.5101	10.1509	11.6372
0.40	60	1680	2.5393	3.6050	10.1509	11.8902
0.32	68	1344	2.5393	3.7631	10.1509	12.2696
0.24	76	1008	2.5393	3.9528	10.1509	12.7756
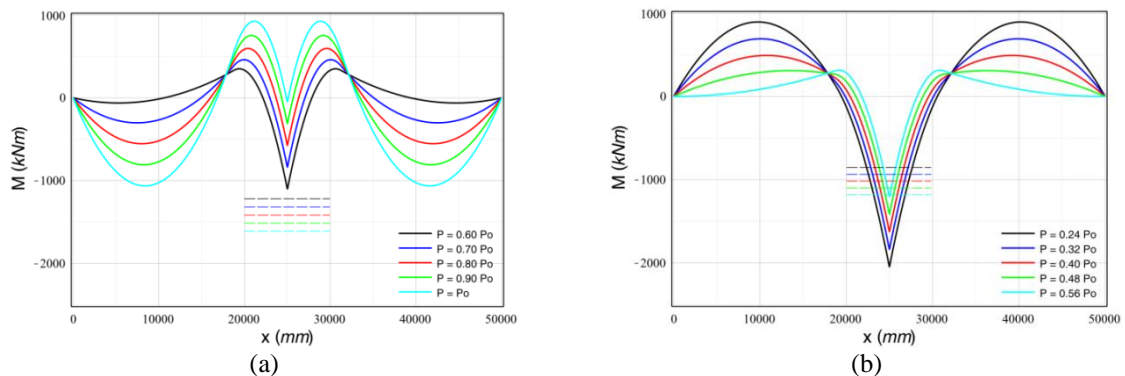
Fig. 17 Case study III – Bending moments (solid lines) and cracking moments (dashed lines) for different values of the prestressing force in the uncracked stage (a) and in the cracked stage (b)

(a)   (b)
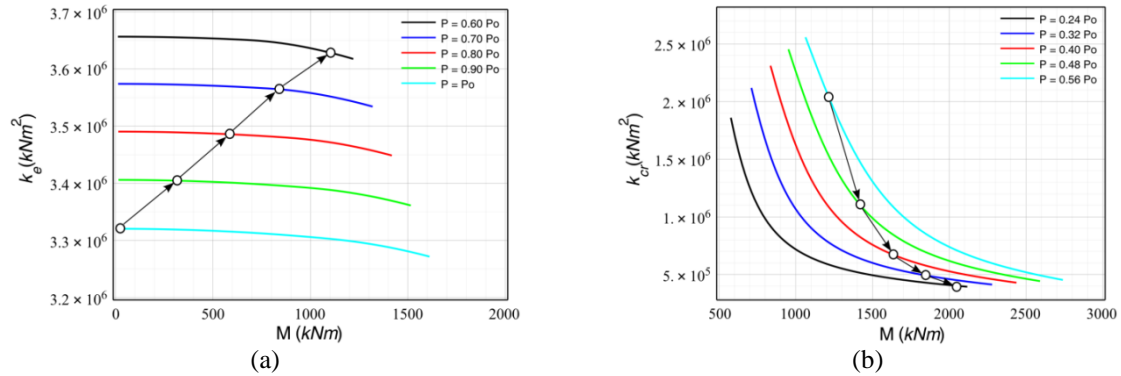
Fig. 18 Case study III - Variation of the flexural stiffness as a function of the bending moment and prestressing force in the uncracked stage (a) and in the cracked stage (b)

(a)   (b)
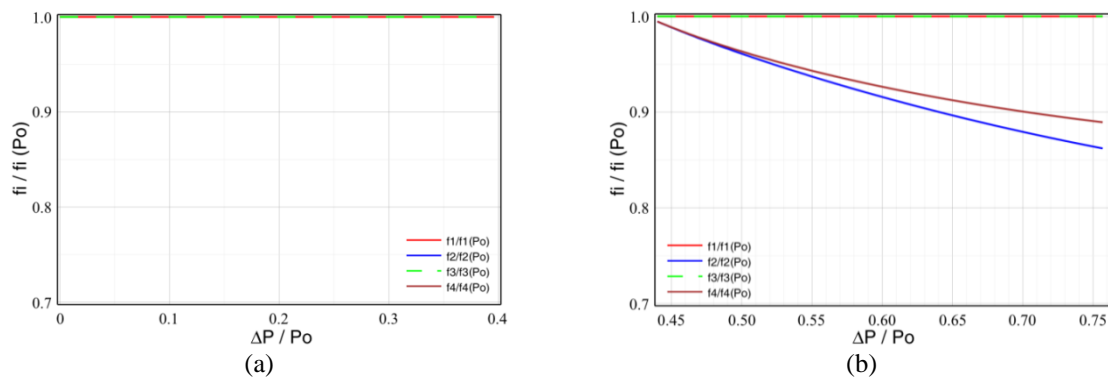
Fig. 19 Case study III - Relative variations of the first 4 frequencies of vibration for decreasing values of the prestress force in the uncracked stage (a) and in the cracked stage (b)

5. Conclusions

The present paper describes a theoretical investigation carried out to evaluate the effect of prestress force on the dynamic properties of continuous PSC beams. In the theoretical consideration, it has been assumed that only the most stressed part of the structure located near the internal support behaves nonlinearly while the other parts of the structure have been considered in the linear elastic state. The nonlinear behaviour takes into account concrete cracking and the nonlinear constitutive law of the concrete in compression. The effect of the prestressing force has been considered twice: in the distribution of the flexural stiffness and in the determination of the moment-curvature relationship. The effective flexural stiffness of the cracked part of the beam has been considered in the evaluation of the dynamic properties (eigenfrequencies and mode shapes) of the continuous PSC beam.

The proposed modelling technique has been applied to three continuous PSC beams case studies with two spans and parabolic strand layouts. Equal and unequal span lengths as well as

different permanent load / total load ratios have been considered to investigate the sensibility of the method. The results of the analysis show that in the uncracked stage, generally observable for small changes to the prestress force, the flexural stiffness of a generic cross section tends to increase with decreasing prestressing force. However, if only the most stressed section behaves nonlinearly while the remaining part of the structure behaves linearly, this phenomenon triggers very limited changes to the overall dynamic properties of the beam.

Much more noticeable is the variation of the frequencies of vibrations detected in the cracked stage for higher changes to the prestress force. In this case, the frequencies of vibration can be reduced by 6% for a prestress reduction of 30%. On the other hand, also mode shapes are influenced by changes to the prestress force but the difficulty of obtaining reliable measures of these figures limits their exploitation.

The results of the investigations also allowed to notice that dynamic techniques can be used to timely detect excessive prestress losses in bridges with high value of the ratio between dead load and total load as occurs, for instance in continuous box girder bridges. It is, also, important to note that this monitoring can be carried out with a limited number of sensors. Conversely, dynamic monitoring turned out to be less effective when dealing with PSC beams with small values of the ration between dead load and total load as happens, for instance, in short span bridges.

References

Breccolotti, M. (2018), "On the evaluation of prestress loss in PRC beams by means of dynamic techniques", *Int. J. Concrete Struct. Mater.*, **12**(1).

Breccolotti, M. and Materazzi, A. (2008), "Identification of a non-linear spring through the Fokker–Planck equation", *Probablist. Eng. Mech.*, **23**, 146-153.

Breccolotti, M., Materazzi, A. and Venanzi, I. (2008), "Identification of the nonlinear behaviour of a cracked RC beam through the statistical analysis of the dynamic response", *Struct. Control Health Monit.*, **15**, 416-435.

CEN (2004), *Eurocode 2: Design of concrete structures - Part 1-1: General rules and rules for buildings*, European Committee for Standardization, Brussels.

Fang, D.P. (2014), "Second order effects of external prestress on frequencies of simply supported beam by energy method", *Struct.Eng. Mech.*, **52**(4), 687-699.

Farrar, C.R. and Jauregui, D.A. (1998), "Comparative study of damage identification algorithms applied to a bridge: I. Experiment", *Smart Mater. Struct.*, **7**(5), 704-719.

Ghosh, S. and Khuntia, M. (2004), "Flexural stiffness of reinforced concrete columns and beams: Analytical approach", *ACI Struct. J.*, **101**(3), 351-363.

Ghosh, S. and Khuntia, M. (2004), "Flexural stiffness of reinforced concrete columns and beams: Experimental verification", *ACI Struct. J.*, **101**(3), 364-374.

Hamed, E. and Frostig, Y. (2004), "Free vibrations of cracked prestressed concrete beams", *Eng. Struct.*, **26**, 1611-1621.

Hamed, E. and Frostig, Y. (2006), "Natural frequencies of bonded and unbonded prestressed beams–prestress force effects", *J. Sound Vib.*, **295**, 28-39.

Huang, C. and Nagarajaiah, S. (2014), "Experimental study on bridge structural health monitoring using blind source separation method: Arch bridge", *Struct. Monit. Maint.*, **1**(1), 69-87.

Huang, M., Liu, J., Law, S. and Lu, Z. (2011), "Vibration analysis of prestressed concrete bridge subjected to moving vehicles", *Interact. Multiscale Mech.*, **4**(4), 273-289.

Kim, B., Jang, J., Lee, H. and Lee, D. (2010), "Effect of prestress force on longitudinal vibration of bonded tendons embedded in a nuclear containment", *Nuclear Eng. Des.*, **240**, 1281-1289.

Li, H., Lv, Z. and Liu, J. (2013), "Assessment of Prestress Force in Bridges Using Structural Dynamic Responses under Moving Vehicles", *Math. Probl. Eng.*, 2013.

Li, H.N., Yi, T.H., Ren, L., Li, D.S. and Huo, L.S. (2014), "Reviews on innovations and applications in structural health monitoring for infrastructures", *Struct. Monit. Maint.*, **1**(1), 1-45.

Limongelli, M., Siegert, D., Merliot, E., Waeytens, J., Bourquin, F., Vidal, R., Le Corvec, V., Gueguen, I. and Cottineau, L.M. (2016), "Damage detection in a post tensioned concrete beam – Experimental investigation", *Eng. Struct.*, **128**, 15-25.

Lundqvist, P. and Rydén, N. (2012), "Acoustoelastic effects on the resonance frequencies of prestressed concrete beams - Short-term measurements", *NDT&E Int.*, **50**, 36-41.

Magnel, G. (1951), "Continuity in prestressed concrete", in Prestressed Concrete Statically Indeterminate Structures, (p. 77-86). (Eds., R. P. Andrew and P. Witt), Cement and Concrete Association.

Naaman, A.E. (2004), *Prestressed Concrete Analysis and Design – Fundamentals*, (Second Ed.), Techno Press 3000, Ann Arbor (USA).

Noble, D., Nogal, M., O'Connor, A. and Pakrashi, V. (2016), "The effect of prestress force magnitude and eccentricity on the natural bending frequencies of uncracked prestressed concrete beams", *J. Sound Vib.*, **365**, 22-44.

Park, R. and Paulay, T. (1975), *Reinforced Concrete Structures*, Wiley, New York.

Remennikov, A.M. and Kaewunruen, S. (2015), "Determination of prestressing force in railway concrete sleepers using dynamic relaxation technique", *J. Perform. Constr. Fac.*, **29**(5).

Smail, M., Waeytens, J. and Bourquin, F. (2014), "The health monitoring of a prestressed concrete beam using inverse modeling technique and measured dynamic response", *Proceedings of the 7th European Workshop on Structural Health Monitoring*, EWSHM 2014. Nantes (F).

Xiang, Z., Chan, T.H., Thambiratnam, D.P. and Nguyen, T. (2016), "Synergic identification of prestress force and moving load on prestressed concrete beam based on virtual distortion method", *Smart Struct. Syst.*, **17**(6), 917-933.

Xuan, F.Z., Tang, H. and Tu, S.T. (2009), "In situ monitoring on prestress losses in the reinforced structure with fiber-optic sensors", *Measurement*, **42**, 107-111.

Zhong, H., Yang, M. and Gao, Z. (2015), "Dynamic responses of prestressed bridge and vehicle through bridge–vehicle interaction analysis", *Eng. Struct.*, **87**, 116-125.

JK